JOURNAL OF SOLID STATE CHEMISTRY 3, 161–171 (1971)

Precipitation of Lithium in Germanium*

GUNTER H. R. KEGEL, BRAHM D. BHARDWAJ†, AND RICHARD J. LARAMEE‡

Lowell Technological Institute, Lowell, Massachusetts 01854

Received July 13, 1970

The precipitation of lithium in solid germanium has been measured: Li is diffused into Ge from an external phase consisting of a molten Li–Pb alloy; diffusion temperatures extend from 250 to 420°C. Precipitation is measured at 60°C. Results are consistent with Morin and Reiss' theory about the nature of precipitation sites and with Ham's theory of diffusion limited precipitation. Measurements of the rate of nuclei generation are in rough agreement with Lothe's theory of vacancy generation by dislocation climb, but are in substantial disagreement with earlier measurements of Morin and Reiss.

Introduction

The solubility of lithium in solid germanium is not large (*1*), it is only 2×10^{15} cm^{-3} at 250°C, but it increases rapidly with temperature and at 500°C it reaches 2×10^{18} cm^{-3}, an increase by a factor of 1000. Hence samples saturated with lithium at an elevated temperature will become supersaturated when the temperature is lowered. This situation is unstable, however, soon precipitates will be formed within the germanium and lithium will diffuse to these precipitate particles, depleting the sample of solute, until supersaturation is eliminated. The present paper refers to this process of precipitation of lithium in germanium.

The main features of the precipitation process have been reported by Morin and Reiss (*2*): Lithium does not precipitate at line defects, such as dislocations, rather lithium precipitation is initiated at point defects which act as precipitation nuclei. Lithium diffuses to these nuclei and forms precipitate particles which grow in size as the precipitation process progresses.

Precipitation is readily measured because dissolved lithium acts as a donor whereas precipitated lithium is electrically inactive. Thus a measurement of electrical conductivity can be used to find the donor concentration and hence the concentration of dissolved Li. Morin and Reiss (*2*) have used this procedure to determine the precipitation rate and thence the concentration and the nature of the precipitation nuclei. They find that spontaneous precipitation is absent and that substitutional lithium atoms act as precipitation nuclei. These are formed by the reaction of a vacancy, □, with an interstitial lithium atom, Li_i to yield a substitutional Li atom, Li_s:

$$Li_i + \square \rightleftharpoons Li_i\,\square = Li_s. \tag{1}$$

The authors were able to determine the equilibrium constant for this reaction

$$K = \frac{N}{VC}. \tag{2}$$

Here C is the concentration of interstitial lithium, V is the vacancy density and N is the concentration of precipitation nuclei. The authors obtain K from the Boltzmann distribution law. If $\Gamma = 4.42 \times 10^{22}$ cm^{-3} is the density of normal lattice sites and if $\epsilon = 1.0$ eV is the energy evolved in reaction (1), then

$$\frac{V}{N} = \frac{\Gamma}{C}\exp(-\epsilon/kT),$$

so that

$$K = \frac{1}{\Gamma}\exp(\epsilon/kT). \tag{3}$$

Morin and Reiss have investigated samples with different dislocation densities; they find that the rate, at which nuclei-vacancies are generated, is proportional to the dislocation density. Since vacancies are generated by the climbing motion of dislocation they proceed to calculate the rate of vacancy generation per length of dislocation.

* Work supported by the Germanium Information Center.

† Present adress: Rice University, Houston, Texas.

‡ Present address: Raytheon Manufacturing Company, Bedford, Massachusetts.

Ham (*3*) has developed a theory of diffusion limited precipitation. According to this theory the average solute concentration $\bar{C}(t)$ is given by

$$\bar{C}(t) - C_s = (C_0 - C_s)\,\Phi(t/\tau), \tag{4}$$

where we can use the following approximation for $\Phi(t/\tau)$

$$\Phi(t/\tau) = \begin{cases} \exp\left\{-\left(\dfrac{t}{n\tau}\right)^n\right\}, & n = \dfrac{3}{2}, \text{ if } \dfrac{t}{\tau} \leqslant \dfrac{3}{2}, \quad (5a) \\ G^* \exp\left\{-\dfrac{t}{\tau}\right\}, & G^* = \sqrt{e}, \text{ if } \dfrac{t}{\tau} \geqslant \dfrac{3}{2}. \quad (5b) \end{cases}$$

Here

$$\tau = \frac{1}{D_L}(4\pi N)^{-2/3}\{(C_0 - C_s)\,3v\}^{-1/3}. \tag{6}$$

The different symbols in Eqs. (4)–(6) have the following meaning:

C_0, the initial solute concentration; C_s, the final solute concentration, i.e. the solubility; D_L, the solute diffusion coefficient; N, the concentration of precipitation nuclei; and v, the inverse of the solute concentration in the precipitate.

Swalin and Weltzin (*4*) have applied Ham's theory to precipitation measurements. They have measured N directly, by electron-microscopic examination. The same technique has also been used to measure v, with the result

$$v = 2.5 \times 10^{-22}\ \text{cm}^{-3}. \tag{7}$$

On the other hand these authors have measured τ and have calculated N. This value is in good agreement with the direct measurement. Swalin and Weltzin find that substitutional oxygen also acts as a precipitation nucleus and they give estimates for the equilibrium constant of the reaction

$$\text{O}_i + \square \rightleftharpoons \text{O}_s \tag{8}$$

We have measured the precipitation of lithium in germanium as a function of time. Our results are essentially in agreement with those previously reported. However, the nuclei-vacancy generation rate which we observe differs drastically from the rate found by Morin and Reiss (*2*).

Sample Preparation

Samples were about 2.7 cm long, 1.0 cm wide and 0.13 cm thick; they were cut from Ga-doped germanium with a resistivity of 10–12 Ω cm. The material had a minority carrier lifetime of 100 μsec, a dislocation density of 1800–1900 pits per cm^2 and it was free from lineage.[1] After cutting, the samples were ground and etched and were plated with tin, using an alkaline plating bath (*5*), in order to facilitate wetting.

TABLE I

DIFFUSION PARAMETERS

Sample	Diffusion temp. (°C)	Diffusion time (hr)	Lithium conc. in sample (cm^{-3})	Lithium conc. in alloy (at %)
P1	285	336	3.8×10^{16}	20.7
P2	250	360	1.02×10^{16}	13.0
P3	330	65	1.08×10^{17}	13.5
P4	360	66	8.0×10^{16}	13.3
P5	390	42	1.12×10^{17}	14.0
P6	420	44	2.6×10^{17}	13.4

Lithium diffusion was carried out by immersing the samples in a molten Li–Pb alloy, at a specified diffusion temperature. For this purpose, a germanium blank and an appropriate amount of Li–Pb alloy were placed in a boat which could be heated in a small oven under vacuum. The oven temperature was regulated; it is estimated that the temperature was constant to ±2°C. The diffusion time and temperature, and the lithium concentration in the sample and in the alloy are given in Table I for all samples. We should add that only samples P1 and P3 were saturated with lithium at the diffusion temperature; all samples were supersaturated at the measuring temperature.

Measurements

After diffusion, samples were etched to remove any Li–Pb alloy; ohmic contacts were applied to the small end faces by grinding and tin plating and finally, the electrical conductivity of the samples was measured in function of time, using a four-contact technique. These measurements were carried out at 60°C.

From the conductivity σ the concentration of dissolved lithium, N_D, was obtained, using the graph of Fig. 1. This conversion is believed to be accurate to 15% for large values of N_D, or for $\sigma \geqslant 0.3\ (\Omega\ \text{cm})^{-1}$. The accuracy is probably worse for $\sigma < 0.3\ (\Omega\ \text{cm})^{-1}$ and fairly large errors will be present if the curve is used near $\sigma = 0.07\ (\Omega\ \text{cm})^{-1}$. The derivation of this curve is given in Appendix B.

[1] Information supplied by the vendors, Sylvania Electric Products, Inc., and Metallurgie Hoboken, Olen, Belgium.

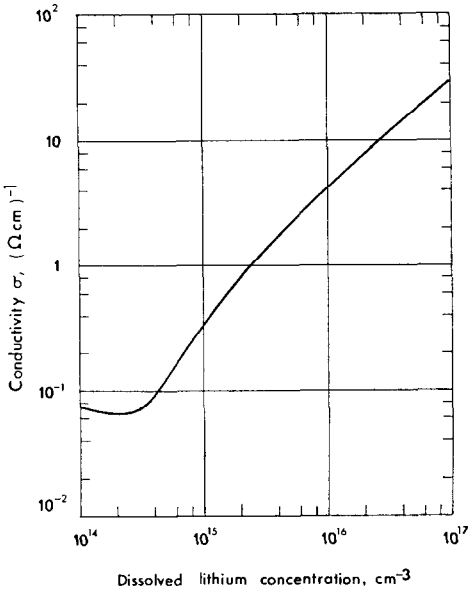

FIG. 1. Sample conductivity versus lithium concentration at 60°C.

Results

Figure 2 shows the precipitation curve for sample P3. In this figure the solid curve represents $C(t)$ as given by Ham, Eq. (4). The parameters of this equation were determined in the following way: The experimental data were plotted; extrapolation to $t = 0$ gave $C(0) = C_0 = 1.08 \times 10^{17}$ cm^{-3}. Next a constant, say c, was subtracted from all measured values. c was varied until all data points with $t > 200$ hr were situated on a straight line, on a graph of $\ln(C(t) - c)$ versus t. A good straight line was obtained for $c = 4.4 \times 10^{14}$ cm^{-3}, this value was taken as C_s. From the slope of the straight line τ was determined, $\tau = 120$ hr.

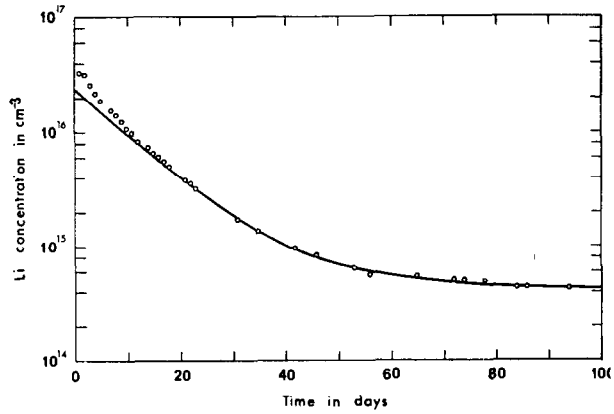

FIG. 3. Precipitation curve for sample P1.

We should point out, at this place, that all samples gave values of C_s between 4×10^{14} cm^{-3} and 4.4×10^{14} cm^{-3}, whereas the lithium solubility for our samples should be 3×10^{14} cm^{-3}. We believe that this difference is not significant and that it is due to the inadequacy of the graph of Fig. 1 near $\sigma = 0.07$ $(\Omega$ cm$)^{-1}$. Precipitation curves for samples P1 and P2 are shown in Figs. 3 and 4 respectively; these samples were diffused at lower temperatures. The initial parts of the curves have a $\exp(t/\tau)^n$ shape but the exponent is 1/2 rather than 3/2 as expected from Eq. (5a). This is illustrated in Fig. 5 which shows a plot of $\ln \bar{C}(t)$ versus $t^{1/2}$.

Swalin and Weltzin (*4*) have observed similar results in their low temperature samples. They suggest that a weak ($\bar{E} \leqslant 0.06$ eV), long range, attractive interaction between dissolved lithium and potential precipitation nuclei is present and

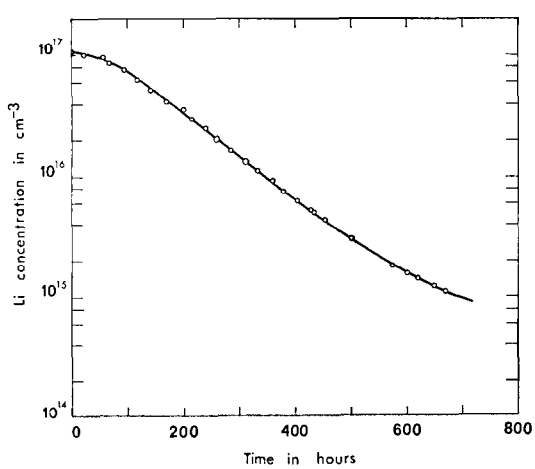

FIG. 2. Precipitation curve for sample P3.

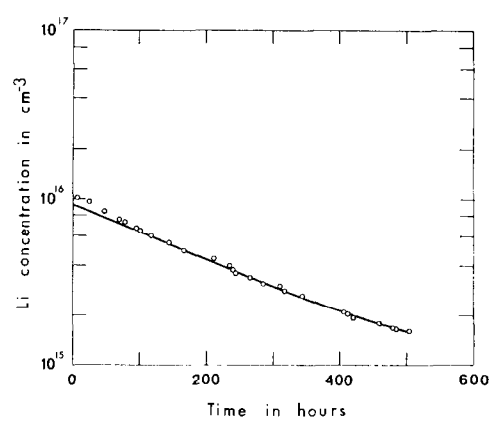

FIG. 4. Precipitation curve for sample P2.

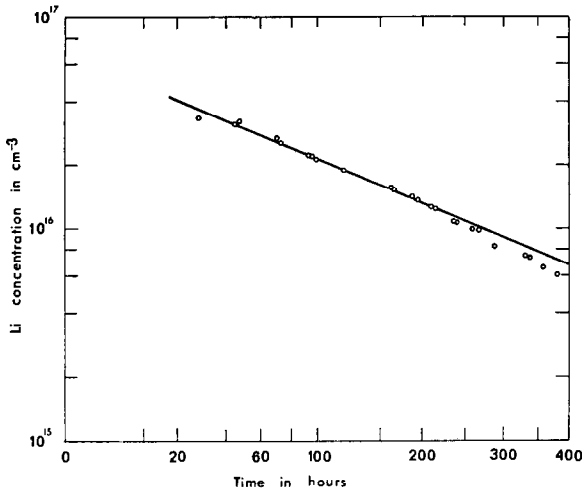

FIG. 5. Precipitation curve for sample P1 : $\ln \bar{C}(t)$ vs $t^{1/2}$.

that this interaction leads to a nonuniform solute distribution. In this case Eqs. (4) and (5) are not applicable; rather a transient, which is usually negligible, is present. This transient is of the form $\exp\{-(t/\tau)^{1/2}\}$.

From the decay parameter τ one can compute the number of precipitation nuclei present in these three samples. The result is shown in Fig. 6; the same figure also shows the saturation number of nuclei as determined by Morin and Reiss (*2*). It is seen that only sample P2 is saturated and that P1 and especially P3 are far from approaching saturation. This result is entirely unexpected because diffusion temperature and duration had been chosen so as to assure saturation with precipitation nuclei.

We have calculated the rate at which nuclei are generated, per cm of dislocation. This rate is shown in Fig. 7, together with the rate reported by Morin and Reiss (*2*). As anticipated our rate for P1 and P3 is smaller by an order of magnitude or more than the rate found by the other authors. This leads us to the tentative conclusion that the mechanism of nuclei generation through motion of dislocations is not as active as expected. Further support for this conclusion is provided by the precipitation data for samples P4, P5 and P6, to be discussed next.

If indeed nuclei generation by dislocation motion is strongly reduced then other processes of nuclei generation should become noticeable. For example, we should expect that some precipitation nuclei are generated by the combination of lithium with those vacancies which have been created at the sample surface and which have reached the sample interior by diffusion. This process has been considered by Morin and Reiss but was found to be of minor importance when compared to vacancy-nuclei generation by dislocation climb.

For our samples this process is not very effective either. It is expected to be largest for sample P6, diffused at 420°C; but even for this sample the

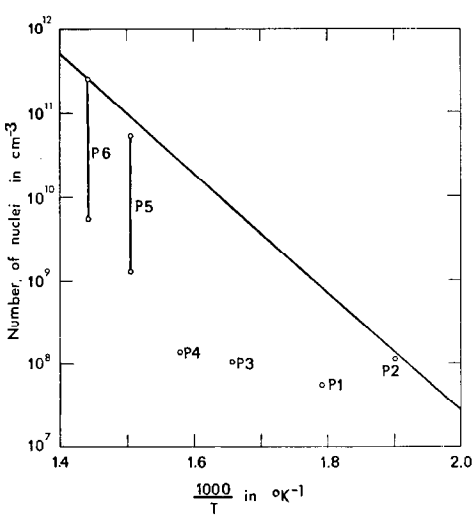

FIG. 6. The number of precipitation nuclei in samples P1–P6 as a function of the diffusion temperature. The solid line represents the saturation number of nuclei as determined by Morin and Reiss (*2*).

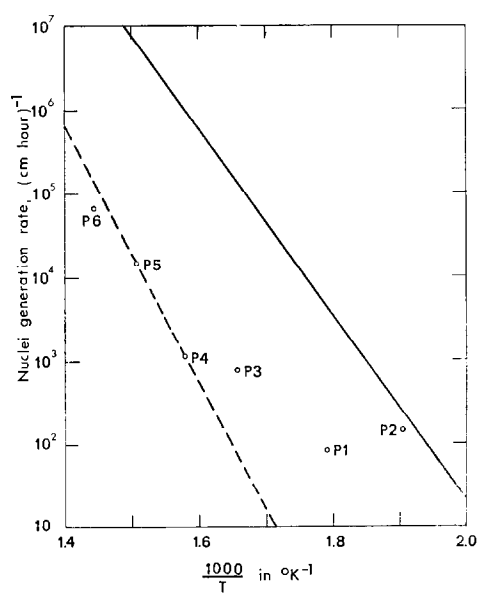

FIG. 7. Nuclei production rate for samples P1 through P6 as a function of the diffusion temperature. The solid line represents the results by Morin and Reiss. The broken line is the theoretical production rate, Eq. (14).

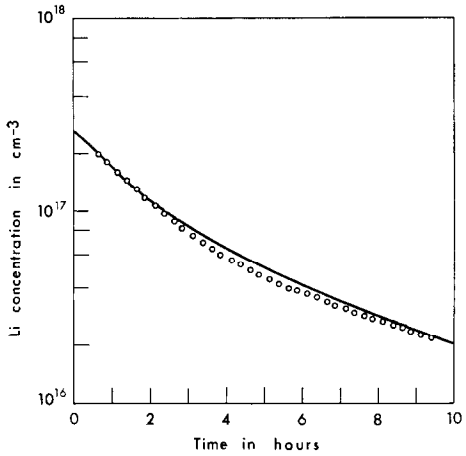

FIG. 8. Precipitation curve for sample P6, initial part.

average depth of vacancy diffusion is only 10^{-2} cm, much less than the sample thickness. In consequence the density of precipitation nuclei will be quite inhomogeneous, the decay parameter τ [Eq. (6)] will become a function of position and the precipitation curve will consist of a superposition of decay curves with different values of τ.

In Appendix A we have analyzed the precipitation curve for sample P6 assuming that (a) the precipitation nuclei are produced by the combination of Li atoms with surface generated vacancies and (b) no nuclei-vacancies are created by dislocation climb. In this case the density of nuclei, $N(x)$, is given by

$$N(x) = N_0 \left\{ \operatorname{erfc} \frac{\frac{a}{2} + x}{2\sqrt{D_v^* \theta}} + \operatorname{erfc} \frac{\frac{a}{2} - x}{2\sqrt{D_v^* \theta}} \right\}. \quad (9)$$

Here N_0 is the surface concentration of nuclei, D_v^* is the vacancy diffusivity, θ is the duration of the diffusion and a is the sample thickness. If we assume that Ham's theory may be applied in this case then the average dissolved lithium concentration $\bar{C}(t)$ can be calculated for any values of N_0 and D_v^*, a and θ being known. A calculated curve which approximates the experimental data fairly well is shown in Figs. 8 and 9. The values of the parameters N_0 and D_v^* of this curve are close to the expected values, thus lending additional support to our assumption about the origin of precipitation nuclei.

The nuclei concentration for sample P6 is indicated in Fig. 6 by a vertical bar which extends from the smallest value of $N(x)$ at $x = 0$ to the largest at $x = a/2$. Since we did not find evidence of dislocation generated nuclei-vacancies in P6, we can only give an upper limit for the rate at which this mechanism proceeds. This limit is indicated in Fig. 7.

Diffusion of sample P5 was carried out at 390°C, at this temperature $D_v^* \simeq 5.4 \times 10^{-10}$ cm^2 sec^{-1}, so

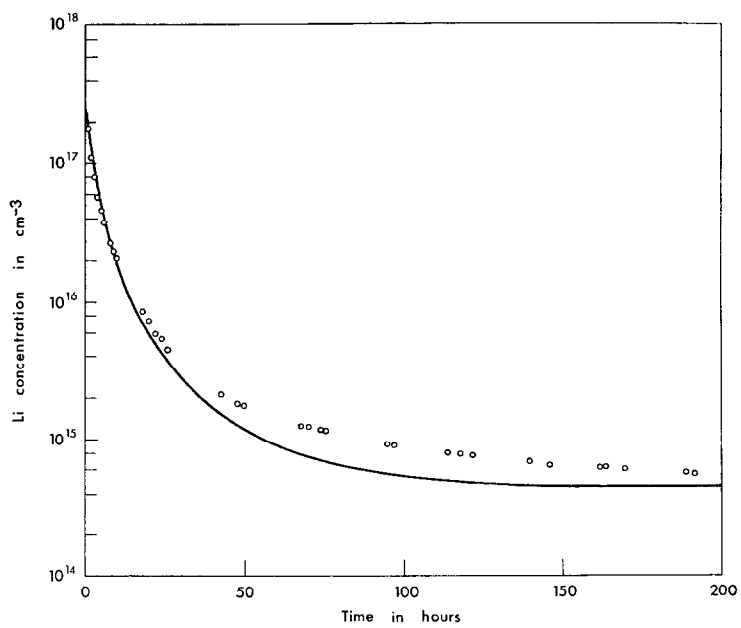

FIG. 9. Precipitation curve for sample P6.

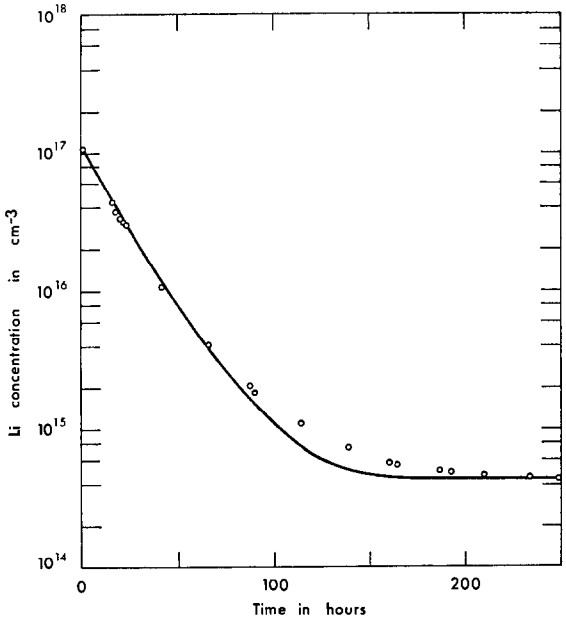

FIG. 10. Precipitation curve for sample P5.

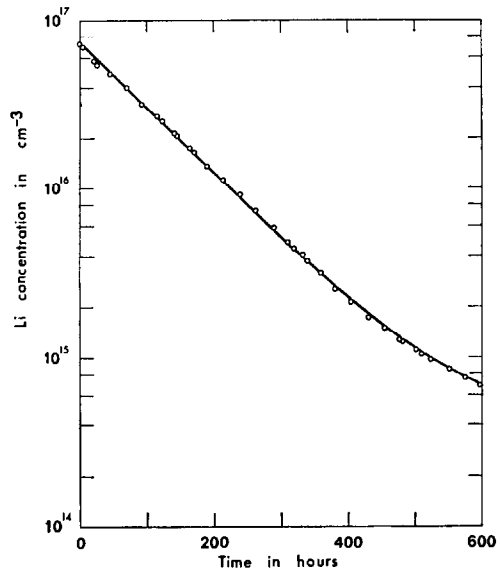

FIG. 11. Precipitation curve for sample P4.

that the center of the sample remains essentially free of surface generated vacancies. Vacancies generated by dislocation climb will predominate in this region so that both processes of vacancy production will have to be taken into account.

The precipitation curve for sample P5 is also analyzed in Appendix A and it is found that 1.4×10^9 cm^{-3} nuclei are generated through dislocation climb. This datum is used to obtain the production rate shown in Fig. 7. Calculated and measured precipitation data for P5 are shown in Fig. 10.

Diffusion of sample P4 was done at still a lower temperature, 360°C. Figure 11 shows that this sample exhibits almost the regular precipitation curve expected from Ham's theory. The initial $\exp\{(t/\tau)^{3/2}\}$-part is missing, though; it is believed that this is due to the presence of a thin layer of nuclei produced by surface generated vacancies. These extra nuclei cause an increased initial precipitation rate, offsetting the slower rate expected from Ham's theory. From the exponential part of the decay curve the decay constant τ is obtained, the number of nuclei is determined, and the rate of nuclei-vacancy generation is computed. These data are included in Figs. 6 and 7.

Discussion

Two topics should be taken up at this time: the presence or absence of impurities and the nuclei generation rate. We consider the impurities first.

Oxygen. According to Swalin and Weltzin (*4*) substitutional oxygen acts as a precipitation nucleus. Since we find nuclei concentrations as low as 10^8 cm^{-3} we conclude the substitutional oxygen concentration cannot exceed this value.

Gallium lithium pairs. Our material contains 3×10^{14} cm^{-3} atoms of gallium; these atoms are expected to form ion pairs of the Li^+Ga^- type (*1*). At the beginning of the precipitation measurements pairing should be almost complete, i.e. there should be no unbound Ga^- in the lattice. Morin and Reiss (*2*) report that Ga^-Li^+ pairs do not act as precipitation nuclei. This is in agreement with our observations: At most 1 in 3×10^6 pairs could act as a precipitation nucleus if all 10^8 cm^{-3} nuclei are assumed to be Ga^-Li^+ pairs.

Boron. The boron content of our samples is small. According to Morin and Reiss (*2*) boron combines with substitutional lithium and forms a complex $Li\square B^-$ which does *not* constitute a precipitation nucleus, so that boron acts as a nucleation inhibitor. In samples P6 and P5 we find nuclei concentrations which approach saturation levels. We would not observe these concentrations if our material contained more than 10^{12} cm^{-3} atoms of boron.

Copper, nickel and silver. These elements have large diffusion coefficients in germanium [see, e.g. (*6*), (*7*)]; trace amounts of them could be present in the Pb–Li alloy used as an external phase for lithium diffusion. We have examined this question in another paper and have found (*8*) that lead should be an effective getter for the removal of

these impurities. This is in agreement with earlier results by Logan and Schwartz (*9*). At 400°C we should obtain a distribution coefficient of about 5×10^{-8} for copper. Thus a copper concentration as high as 100 ppm in the lead would be in equilibrium with only 2×10^{11} cm^{-3} of Cu in the Ge samples. Similar results apply to nickel and silver and possibly to cobalt and iron.

Iron. Iron has been used in the alloy preparation and during the diffusion and quite possibly it is present in the external phase. The solubility of iron is quite small, though, both in liquid lead (*10*) and in solid germanium (*11*). Furthermore the Fe diffusivity in Ge is small (*6*). These arguments lead us to believe that Fe is not an important impurity in our samples.

Others. An unidentified impurity is probably present in sample P2 and possibly P1. Figure 6 shows that P2 is saturated with precipitation nuclei. This could be due to an excessively long diffusion interval. In that case the rate as shown in Fig. 7 should be quite low and this is not found. Possibly another type of precipitation nucleus is present in P2 but further measurements are needed to confirm this hypothesis.

We now turn our attention to the rate of vacancy generation, Fig. 7, where we have a large difference between our data and those of Morin and Reiss. These authors have found that trace amounts of boron reduce the number of precipitation nuclei appreciably. This reduction should affect both, the nuclei generation rate and the saturation concentration of the nuclei. In sample P6 we measure a nuclei concentration which is very close to saturation, hence is unaffected by boron, and we conclude that our generation rate too should be unaffected by boron.

A variety of arguments may be presented in an attempt to explain our low generation rate: For example, lead diffusion might cause dislocation pinning at the sample surface inhibiting jog formation. Other plausible arguments are readily found. It seems worthwhile therefore, to examine the kinetics of vacancy generation and to check if our results are consistent with current theories.

The following description is usually given of the vacancy generation by dislocation climb (*12*, *13*): Jogs are created at the point where the dislocation intercepts the sample surface; they travel along the dislocation leaving trails of vacancies behind. Lothe (*14*) has examined the jog propagation in more detail. He proposes that vacancies diffuse preferentially along the dislocation and evaporate into the lattice from the dislocation but not from the jog directly. The rate of vacancy generation depends then on the ability of the lattice to absorb vacancies.

If either the number of jogs is large or if the diffusivity along the dislocation is large then a saturation condition develops: The dislocation in its entire length acts as a line source of vacancies and the rate of vacancy generation is obtained by solving the boundary value problem of vacancy diffusion. There is of course no assurance that this saturation condition applies to our samples. It is seen, however, that the saturation condition leads to the largest possible vacancy generation rate. We shall show that this rate is in rough agreement with our results but is in disagreement with the data by Morin and Reiss.

The boundary value problem to be solved is the following: At the dislocation surface ($r = b$) the vacancy concentration is equal to the vacancy solubility, $V(b) = V_{sat}$; at a large distance, R, a much smaller vacancy concentration $V(R) = V_R$ is present. In the steady state

$$V(r) = \frac{\rho}{2\pi} \ln \frac{r}{R} + V_R, \tag{10}$$

where

$$\rho = \frac{2\pi(V_{sat} - V_R)}{\ln R - \ln b}. \tag{11}$$

The rate of vacancy generation is

$$g = 2\pi r D_v \frac{\partial V}{\partial r} = D_v \rho \simeq \frac{2\pi D_v V_{sat}}{\ln \frac{R}{b}}. \tag{12}$$

This result may be simplified by introducing the self-diffusion coefficient for Ge, D_s

$$D_s = \frac{D_v V_{sat}}{\Gamma}, \tag{13}$$

where Γ has the same meaning as in Eq. (3). We obtain

$$g = \frac{2\pi \Gamma D_s}{\ln \frac{R}{b}}. \tag{14}$$

This rate is not strongly dependent on R or b. We take $b = 5 \times 10^{-8}$ cm and we take R equal to one-half of the average separation between adjacent dislocations, $R = 10^{-2}$ cm. D_s has been measured by Letaw, et al. (*15*) so that g as given by Eq. (14) is known. This function is shown as a broken line in Fig. 7, and is seen to be in rough agreement with our results.

Appendix A

In this appendix we consider the following question: Lithium ions and vacancies diffuse from the surface into the germanium sample. What is the resultant distribution of precipitation nuclei and what is the form of the ensuing precipitation process? Similar problems have been considered by Frank and Turnbull (*16*) and by Kegel (*17*). If we denote by $C(x, t)$, $V(x, t)$ and $N(x, t)$ the concentrations of lithium, of vacancies, and of precipitation nuclei, respectively, then we have [Eqs. (3), (4) of (*17*)]

$$\frac{\partial C}{\partial t} = D_L \frac{\partial^2 C}{\partial x^2} - \frac{\partial N}{\partial t}, \tag{15}$$

$$\frac{\partial V}{\partial t} = D_v \frac{\partial^2 V}{\partial x^2} - \frac{\partial N}{\partial t} + G - \alpha V, \tag{16}$$

$$N = KCV. \tag{17}$$

Here D_L and D_v are the diffusion coefficients of lithium and of vacancies, respectively. G and αV are the rates at which vacancies are generated and absorbed by the motion of dislocations within the crystal. The orientation of the x direction is shown in Fig. 12. Diffusion into the sample along the y and z directions is neglected, because the interior of the sample is too far away from the surfaces $y = \text{const}$ and $z = \text{const}$.

In the present case we shall neglect generation and absorption of vacancies by motion of dislocations, i.e. we shall put $G = \alpha = 0$ in (16). Before integrating the two differential equations two points should be noted. First, D_L is larger than D_v; for $T = 420°\text{C}$ (sample P6) we have

$$D_L = 4.9 \times 10^{-7}\ \text{cm}^2\ \text{sec}^{-1}, \tag{18}$$

$$D_v = 1.2 \times 10^{-7}\ \text{cm}^2\ \text{sec}^{-1}. \tag{19}$$

Secondly, the initial lithium concentration in P6, $C_0 = 2.6 \times 10^{17}\ \text{cm}^{-3}$ exceeds by a large factor the saturation concentration of precipitation nuclei, N_{sat} (*2*),

$$N_{\text{sat}} = 3.4 \times 10^{11}\ \text{cm}^{-3}, \tag{20}$$

which in turn is larger than the saturation concentration of vacancies, [see, e.g. Mayburg (*18*)]

$$V_0 = 7.3 \times 10^8\ \text{cm}^{-3}. \tag{21}$$

In consequence the loss of Li ions due to the formation of precipitation nuclei should hardly affect the lithium concentration, whereas the loss of vacancies due to the same process should drastically slow down the net diffusion of vacancies into the sample. Thus the Li diffusion is much faster than that of the vacancies, so that we can use the following approximations:

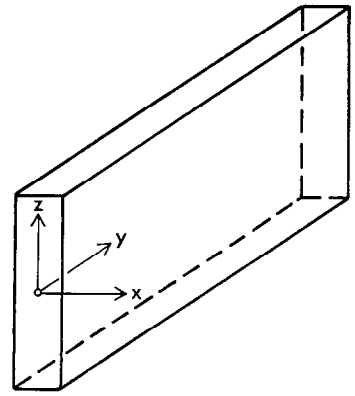

FIG. 12. Sample geometry. The electric current flows in the y direction.

In the differential equation for $C(x, t)$ we neglect the $\partial N/\partial t$ term and in the equation for $V(x, t)$ we assume that $C(x, t) = \text{const} = C_0$ since $C(x, t) \simeq C_0$ wherever $V(x, t)$ differs markedly from zero.

With these approximations the differential equation (16) takes the form

$$\frac{\partial V}{\partial t} = \frac{D_v}{1 + KC_0} \frac{\partial^2 V}{\partial x^2} = D_v^* \frac{\partial^2 V}{\partial x^2}. \tag{22}$$

Here we have introduced the effective diffusion coefficient D_v^* [see, e.g., (*19*, Eq. (6.53))]

$$D_v^* = \frac{D_v}{1 + KC_0}. \tag{23}$$

For P6, $KC_0 \simeq 110$, so that indeed $D_v^* \ll D_v$ as our arguments indicated.

The boundary conditions, applicable to (22), are

$$V\left(\frac{a}{2}, t\right) = V\left(-\frac{a}{2}, t\right) = V_0, \tag{24}$$

and the solution is

$$V(x, t) = V_0 \left\{ \operatorname{erfc} \frac{\frac{a}{2} + x}{2\sqrt{D_v^* t}} + \operatorname{erfc} \frac{\frac{a}{2} - x}{2\sqrt{D_v^* t}} \right\}. \tag{25}$$

The boundary conditions are met,

$$V\left(\pm\frac{a}{2}, t\right) = V_0 \left\{ 1 + \operatorname{erfc} \frac{a}{2\sqrt{D_v^* t}} \right\} \simeq V_0, \tag{26}$$

because even for the largest value of t, $t = \theta = 44$ hr, the argument of erfc is 3.5 and erfc 3.5 is negligibly small. From $V(x, t)$ we obtain $N(x, t)$, and more specifically $N(x, \theta)$, the density of precipitation

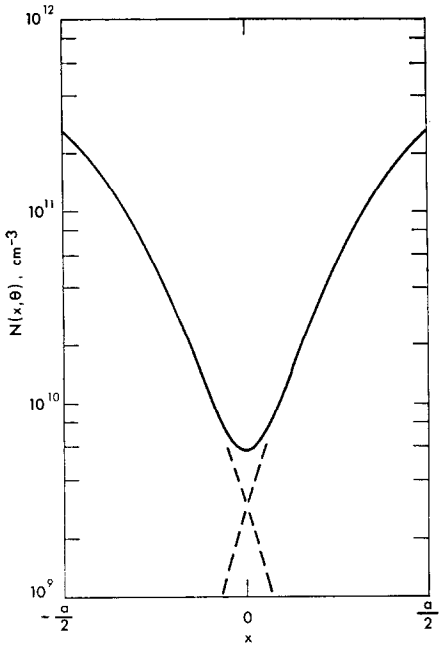

FIG. 13. Concentration of precipitation nuclei $N(x, \theta)$, versus x, Eq. (27).

nuclei at the end of the diffusion cycle, i.e. for $t = \theta$

$$N(x, \theta) = KC_0 V(x, \theta) = N_0 \left\{ \operatorname{erfc} \frac{\frac{a}{2} + x}{2\sqrt{D_v^* \theta}} + \operatorname{erfc} \frac{\frac{a}{2} - x}{2\sqrt{D_v^* \theta}} \right\}. \tag{27}$$

This function is shown in Fig. 13. It is seen that N is quite small for $x = 0$. Thus precipitation in the centre of the sample will be slow. This allows us to use an approximation suitable for the early phase of the precipitation process: We retain only one of the two erfc terms in (25); for $x \geqslant 0$ we have

$$N(x, \theta) \simeq N_0 \operatorname{erfc} \frac{\frac{a}{2} - x}{2\sqrt{D_v^* \theta}}. \tag{28}$$

We turn our attention to the precipitation process now. Since N is a function of x, τ will depend on x too. For our computations the inverse, η, is more convenient. We have, combining (6) and (28)

$$\eta(x) = \frac{1}{\tau(x)} = D_L (4\pi N)^{2/3} (3(C_0 - C_s) v)^{1/3}, = \eta_0 \psi(u), \tag{29}$$

where

$$\eta_0 = D_L (4\pi N_0)^{2/3} (3(C_0 - C_s) v)^{1/3}, \tag{30}$$

$$\psi(u) = (\operatorname{erfc} u)^{2/3}, \tag{31}$$

$$u = \frac{\frac{a}{2} - x}{2\sqrt{D_v^* \theta}}. \tag{32}$$

The lithium concentration at x is

$$C(x, t) - C_s = (C_0 - C_s) \Phi(\eta(x) t). \tag{33}$$

The conductivity corresponding to this concentration is obtained from Fig. 1,

$$\sigma = \sigma(C(x, t)). \tag{34}$$

The average conductivity $\bar{\sigma}$ is determined by our measurements; this quantity is

$$\bar{\sigma} = \frac{1}{a} \int_{-a/2}^{+a/2} \sigma(C(x, t))\, dx. \tag{35}$$

At this point it is again convenient to simplify matters through the use of an approximation. We expand $\sigma(C(x, t))$ in powers of $C(x, t) - \bar{C}(t)$, being the average lithium concentration

$$\sigma(C(x,t)) = \sigma(\bar{C}(t)) + (C(x,t) - \bar{C}(t)) \frac{d\sigma}{dC}(\bar{C}(t)) + \tfrac{1}{2}(C(x,t) - \bar{C}(t))^2 \frac{d^2\sigma}{dC^2}(\bar{C}(t)) + \ldots. \tag{36}$$

If we average over x we obtain

$$\bar{\sigma} = \sigma(\bar{C}(t)) + \frac{1}{2} \frac{d^2\sigma}{dC^2}(\bar{C}(t)) \frac{1}{a} \int_{-a/2}^{a/2} (C(x,t) - \bar{C}(t))^2\, dx + \ldots. \tag{37}$$

The approximation we propose to use consists in omitting the second-order term as well as all higher-order terms in this equation. The error introduced in this way amounts to a few percent, only, because of the following: For t equal to 1 or 2 hr the integral has its maximum, but $d^2\partial/dC^2$ is small, as Fig. 1 shows. On the other hand for $C \simeq 10^{15}$ cm^{-3}, $d^2\sigma/dC^2$ becomes large, but in this case the integral is quite small. With this approximation, (37) reduces to

$$\bar{\sigma} = \sigma(\bar{C}(t)), \tag{38}$$

so that $\bar{C}(t)$ can be obtained in a straightforward way from $\bar{\sigma}$, using Fig. 1. This function can be written as

$$\bar{C}(t) - C_s = (C_0 - C_s)\frac{2}{a}\int_0^{a/2} \Phi(\eta_0\, t\psi(u))\, dx, \tag{39}$$

$$= (C_0 - C_s)\frac{1}{U}\int_0^{U} \Phi(\eta_0\, t\psi(u))\, du,$$

where

$$U = \frac{a}{4\sqrt{D_v{}^*\theta}}. \tag{40}$$

In this equation η_0 appears as a scale factor which compresses or expands the time scale. This variability can be suppressed by normalizing the time scale. Select $t = \vartheta$ so that

$$\bar{C}(\vartheta) - C_s = \tfrac{1}{2}(C_0 - C_s) \tag{41}$$

and introduce a new variable w by

$$t = \vartheta w, \tag{42}$$

finally write

$$\frac{\bar{C}(\vartheta w) - C_s}{C_0 - C_s} = \zeta_{\text{calc}}(w), \tag{43}$$

then $\zeta_{\text{calc}}(0) = 1$, $\zeta_{\text{calc}}(1) = 0.5$. ζ_{calc} is a function of the independent variable w and contains only one adjustable parameter, U. This function has been computed for various values of U by numerical integration of (39).

A function $\zeta_{\text{meas}}(w)$ has been obtained from the experimental data for P6. This function is best approximated by a $\zeta_{\text{calc}}(w)$ with $U = 1.8$. For this ζ_{calc}, $\eta_0\vartheta = 3.45$ and for ζ_{meas}, $\vartheta = 1.64$ hr; these two values give $\eta_0 = 2.09$ hr^{-1}. η_0 and U are used to compute N_0 and $D_v{}^*$, using (30) and (40),

$$N_0 = 2.64 \times 10^{11}\ \text{cm}^{-3} \tag{44}$$

$$D_v{}^* = 1.13 \times 10^{-9}\ \text{cm}^2\ \text{sec}^{-1}. \tag{45}$$

The value of N_0 is somewhat larger than expected. Sample P6 contains only $C_0 = 2.6 \times 10^{17}$ cm^{-3} atoms of Li, about 40% of the saturation value at the diffusion temperature, $C_{\text{sat}} = 6.3 \times 10^{17}$ cm^{-3}. According to Eq. (17) we should expect that

$$N_0 \simeq \frac{C_0}{C_{\text{sat}}} N_{\text{sat}} = 1.4 \times 10^{11}\ \text{cm}^{-3}. \tag{46}$$

There does not seem to be any obvious reason for the discrepancy between observed and expected values.

The agreement is much better as far as $D_v{}^*$ is concerned. At 420°C the vacancy diffusion coefficient is [see, e.g. Letaw, et al. (*15*)]

$$D_v = 1.2 \times 10^{-7}\ \text{cm}^2\ \text{sec}^{-1}, \tag{47}$$

and since $KC_0 \simeq 110$ we should find

$$D_v{}^* = 1.1 \times 10^{-9}\ \text{cm}^2\ \text{sec}^{-1} \tag{48}$$

which is in good agreement with the measured value (45).

We return to $\zeta_{\text{calc}}(w)$ now. We use this function together with $U = 1.8$ and $\eta_0 = 2.09$ hr^{-1} to obtain $\bar{C}(t)$ as determined by (43) and (39). This function is shown in Figs. 8 and 9.

In principle the data of sample P5 can be analyzed in the same fashion as those of P6. However, since P5 was diffused at a lower temperature, (390°C), the generation of vacancies by dislocation climb is no longer negligible. For this reason we write the nuclei density $N(x)$ as

$$N(x) = N_1(x) + N_2. \tag{49}$$

Here

$$N_1(x) = N_{10}\left\{\text{erfc}\frac{\frac{a}{2} + x}{2\sqrt{D_v{}^*\theta}} + \text{erfc}\frac{\frac{a}{2} - x}{2\sqrt{D_v{}^*\theta}}\right\} \tag{50}$$

represents nuclei created with surface-generated vacancies and N_2 represents nuclei generated via dislocation climb. The experimental results for P5 are not detailed enough to allow for the determination of the three unknowns, N_{10}, N_2 and $D_v{}^*$, in (49). For this reason we use eq. (17) to obtain N_{10} with $K = 9.5 \times 10^{-16}$ cm^3 [Eq. (3)] and $C_0 = 1.12 \times 10^{17}$ cm^{-3}. For V we use the value obtained from P6, corrected for the different diffusion temperature. This gives us $N_{10} = 5.4 \times 10^{10}$ cm^{-3}. $D_v{}^*$ is calculated from Eq. (23) using the vacancy diffusion coefficient of Letaw, et al. (*15*), with the result $D_v{}^* = 5.4 \times 10^{-10}$ cm^2 sec^{-1}. N_2 finally, is selected so as to optimize agreement between calculated and measured precipitation curves for P5. This criterion leads to $N_2 = 1.4 \times 10^9$ cm^{-3}. Calculated and measured data are shown in Fig. 10.

Appendix B

In this appendix we determine the sample conductivity σ in function of the dissolved lithium concentration, N_D.

The conductivity σ is

$$\sigma = e(n\mu_n + p\mu_p). \tag{51}$$

Here n and p are the concentrations of electrons and holes respectively and the two μ's are the mobilities. All four parameters are functions of the dissolved lithium concentration, therefore this quantity can be found once σ is known.

According to Reiss, Fuller, and Morin (*1*) the concentrations of electrons and holes and of Ga^- and Li^+ are governed by the following set of equilibrium reactions

$$\begin{array}{ccccc} Li & \rightleftharpoons & Li^+ & + & e^- \\ & & + & & + \\ Ga & \rightleftharpoons & Ga^- & + & e^+ \\ & & \Updownarrow & & \Updownarrow \\ & & Li^+Ga^- & & e^-e^+. \end{array} \tag{52}$$

At the measuring temperature both, gallium and dissolved lithium are almost completely ionized. The electron and hole concentrations are related by

$$np = \{n_i(T)\}^2. \tag{53}$$

Morin and Maita (*20*) have measured $n_i(T)$; at 60°C, $n_i = 10^{14}$ cm^{-3}. The equilibrium constant of the reaction

$$Li^+ + Ga^- \rightleftharpoons Li^+Ga^- \tag{54}$$

has been calculated by Reiss, Fuller, and Morin (*1*)

$$\frac{P}{A^- D^+} = \Omega. \tag{55}$$

Here P is the concentration of Li^+Ga^- pairs; A^- and D^+ are concentrations of gallium and lithium ions, respectively. At 60°C, Ω is approximately 4×10^{-16} cm^3. The total gallium concentration N_A is related to A^- by

$$N_A = A^- + P. \tag{56}$$

A similar relation holds for the dissolved lithium concentration,

$$N_D = D^+ + P. \tag{57}$$

Equations (53), (55), (56) and (57) together with the condition of electrical neutrality

$$D^+ + p = A^- + n \tag{58}$$

form a system of equations for the determination of n, p, P, A^- and D^+ as functions of N_D, N_A being equal to 3×10^{14} cm^{-3}. Finally hole and electron mobilities are computed using the results of Debye and Conwell (*21*). The mobilities and the electron and hole concentrations are used to obtain σ; the result is shown in Fig. 1.

References

1. H. Reiss, C. S. Fuller, and F. J. Morin, *Bell Syst. Tech. J.* **35**, 535 (1956).
2. F. J. Morin and H. Reiss, *J. Phys. Chem. Solids* **3**, 196 (1957).
3. F. S. Ham, *J. Phys. Chem. Solids* **6**, 335 (1958).
4. R. A. Swalin and R. D. Weltzin, *Progr. Solid State Chem.* **2**, 175 (1965).
5. J. B. Mohler and H. J. Sedusky, "Electroplating for the Metallurgist, Engineer and Chemist," Chemical Publishing Co., Inc., New York, 1951.
6. U. Gurs and K. Gurs, *in* "Landolt-Bornstein Zahlenwerte und Funktionen," (H. Borchers and E. Schmidt, Eds.), vol. 2c, p. 734, Springer-Verlag, Berlin, 1965.
7. V. E. Kosenko, *Fiz. Tverd. Tela* **4**, 59 (1962); *Fiz. Tverd. Tela* **3**, 2102 (1961).
8. G. H. R. Kegel, *in* "Symposium on Semiconductor Detectors for Nuclear Radiation," Munich, May 1970, p. 35, P. Eichinger and G. Keil, Munich, 1970.
9. R. A. Logan and M. Schwartz, *J. Appl. Phys.* **26**, 1287 (1955).
10. M. Hansen and K. Anderko, "Constitution of Binary Alloys," McGraw-Hill, New York, 1958; R. P. Elliot, "Constitution of Binary Alloys, First Supplement," McGraw-Hill, New York, 1965; F. A. Shunk, "Constitution of Binary Alloys, Second Supplement," McGraw-Hill, New York, 1969.
11. F. A. Trumbore, *Bell Syst. Tech. J.* **39**, 416 (1960).
12. J. P. Hirth and J. Lothe, "Theory of Dislocations," McGraw-Hill, New York, 1968.
13. J. Friedel, "Dislocations," Addison Wesley, Reading, Mass., 1964.
14. J. Lothe, *J. Appl. Phys.* **31**, 1077 (1960).
15. H. Letaw, W. M. Portnoy, and L. Slifkin, *Phys. Rev.* **102**, 636 (1956).
16. F. C. Frank and D. Turnbull, *Phys. Rev.* **104**, 617 (1956).
17. G. H. R. Kegel, *IEEE Trans. Nucl. Sci.* **15**, 332 (1968).
18. S. Mayburg, *Phys. Rev.* **95**, 38 (1954).
19. H. Reiss and C. S. Fuller, *in* "Semiconductors," (N. B. Hanney, Ed.), Reinhold Publ. Co., New York, 1959.
20. F. J. Morin and J. P. Maita, *Phys. Rev.* **94**, 1525 (1954).
21. P. P. Debye and E. M. Conwell, *Phys. Rev.* **93**, 693 (1954).